The Ordered K$_2$NiF$_4$-type Structure of Mixed Crystals La$_{2-x}$Sr$_x$Li$_{1/2}$Co$_{1/2}$O$_4$ ($x < 0.5$) and the Electronic Properties of the Constituting Co^{III} and Co^{IV} Ions

Salam A. Warda, Werner Massa, and Dirk Reinen[1]

Fachbereich Chemie und Zentrum für Materialwissenschaften der Philips-Universität, Hans-Meerwein-Straße, D-35032 Marburg, Germany

Zhiwei Hu and Günter Kaindl

Institut für Experimentalphysik, Freie Universität Berlin Arnimalle 14, D-14195 Berlin-Dahlem, Germany

and

Frank M. F. de Groot

Solid State Physics, University of Groningen, 9747 AG Groningen, The Netherlands

 Solids of the composition La$_{2-x}$Sr$_x$Li$_{1/2}$Co$_{1/2}$O$_4$ ($x = 0$, $x \cong 0.2$) crystallize in a superstructure of the K$_2$NiF$_4$ lattice with a doubled unit cell in the (001) plane (space group *Ammm*; $a = b = \sqrt{2}a_0$), caused by cation ordering between lithium and cobalt on the octahedral sites. The electronic structure of the Co^{III}O$_6$ and Co^{IV}O$_6$ polyhedra, which lie isolated in the lattice, were studied by various spectroscopic techniques (XANES, EPR, optical). The groundstates are low-spin in both cases (t_{2g}^6 and t_{2g}^5, respectively), the ligand field parameters of Co^{III} being close to those characterizing the high-spin/low-spin crossover. © 1999 Academic Press

I. INTRODUCTION

We have recently determined the structure of the solids La$_2$Li$_{1/2}$M$_{1/2}$O$_4$ (M^{III} = Co, Ni, Cu) by single crystal X-ray analysis and analyzed the electronic properties of the trivalent M^{III} cations by means of EPR and optical (1) as well as XANES spectroscopy (2). The unit cell is of the K$_2$NiF$_4$-type, but corresponds to a superstructure of this lattice in the (001) plane with $a = b = a_0\sqrt{2}$ (Fig. 1). It is caused by cation ordering between Li and M on the octahedral sites, the space group being *Ammm* (orthorhombic, No. 65). However, diffuse streaks along c^* are frequently observed in addition, which indicate order–disorder effects

in the stacking sequence along c. The M^{III} cations—isolated from each other due to the cation ordering—are low-spin configurated; the Ni^{III}O$_6$ octahedra display the distinct tetragonal elongation characteristic of the Jahn–Teller effect, and Cu^{III} possesses the typical square-planar coordination of covalent d^8 cations (with two additional long-bonded oxygen atoms). The covalency of the M^{III}–O bond increases from Co^{III} via Ni^{III} to Cu^{III}. Using a molecular orbital description in O$_h$ for the antibonding e_g^* electrons d_z^2 and $d_{x^2-y^2}$ involved in the M^{III}–O overlap, we obtain the expression (1) for the ground state MO, where $L(e_g)$ is the symmetry-adapted LCAO of the oxygen ligands:

$$\Psi_g^* = \alpha e_g - \beta L(e_g). \qquad [1]$$

The mixing coefficient is $\alpha \approx 0.9$ for Ni^{III} ($t_{2g}^6 e_g^1$), indicating a rather ionic bond with still about 80% of the e_g^* electron density present at the metal. This number decreases to $\approx 65\%$ ($\alpha \approx 0.8$) for Cu^{III} (2).

It is also possible to stabilize the oxidation state ($+$IV) in this type of oxide ceramics in the case of cobalt. Mixed crystals La$_{2-x}$Sr$_x$Li$_{1/2}$Co$_{1/2}$O$_4$ ($0 \leq x \leq 0.5$) have been described (3) where the end member La$_{1.5}$Sr$_{0.5}$Li$_{1/2}$Co$_{1/2}^{IV}$O$_4$, however, can only be prepared under oxygen pressure. Mixed phases up to $x \approx 0.2$—with about 40% Co^{IV} and 60% Co^{III}—are obtainable as single crystals under flowing oxygen, and we have performed an X-ray structure determination for this composition. The electronic properties of

[1]To whom correspondence should be addressed.

the two valence states were studied by EPR and XANES spectroscopy.

II. EXPERIMENTAL

Synthesis

Powder samples of $La_{2-x}Sr_xLi_{1/2}Co_{1/2}O_4$ with $x \cong 0.2$ were prepared according to the experimental procedures described in Ref. (1), using a mixture of $La(OH)_3$, $SrCO_3$, Co_3O_4, and $LiCO_3$. Brownish black single phase products result. The average oxidation state has been determined by iodometric titration, the resulting value of 3.4(1) being in accord with the X-ray and XANES results.

Single crystals were obtained from a LiOH melt. A stoichiometric mixture of $La_{1.8}Sr_{0.2}Li_{1/2}Co_{1/2}O_4$ was heated to 1073 K and held at this temperature for 20 h. Well-shaped black prismatic and plate-like crystals grew during the cooling process with a rate of 20 K/h. Both kinds of crystals were used for film exposures and data collection. The plates proved to be more suitable for structural studies, because the observed diffuse streaks were weaker than in the case of the prismatic crystals.

X-Ray Spectroscopy

The XANES (X-ray absorption near-edge structure) measurements were performed at the SX700/II monochromator operated by the Freie Universität Berlin at the Berliner Elektronenspeicherring für Synchrotronstrahlung (BESSY). For the XANES studies at the oxygen $K(1s)$ edge the fluorescence-yield mode was used, while the spectra at the cobalt $L_3(2p_{3/2})$ and $L_2(2p_{1/2})$ edges were recorded via total electron yield. The energy scale was calibrated using the known peak positions of the OK and CuL edges in CuO. At the OK and CuL_3 thresholds, the experimental resolution was 0.3 and 0.5 eV, respectively. The samples were scraped in the experimental UHV chamber, which had a base pressure of $\cong 1 \times 10^{-10}$ mbar.

EPR and Optical Spectroscopy

EPR measurements were performed at X and Q band frequencies in the temperature range between 300 and 4 K with a Bruker ESP-300 spectrometer. UV-VIS spectra were recorded using the powder diffuse reflection technique with a Zeiss PMQII spectrometer.

X-Ray Diffraction Analysis

X-ray investigations were performed on single crystals using a precession camera (Enraf-Nonius, Mo$K\alpha$ radiation), a 4-circle diffractometer (CAD4, Nonius), and for the final data recording an IPDS (Stoe) area detector system (both using Mo$K\alpha$ radiation and a graphite monochromator).

A careful numerical absorption correction was applied after optimization of the distances of the indexed crystal faces (4). The film records as well as the IPDS images revealed, besides the strong and sharp reflections of the basic K_2NiF_4 lattice superstructure, reflections indicating a doubling of the unit cell in the (001) plane according to $a = b = a_0\sqrt{2}$, $c = c_0$ (Fig. 1). Like in the $La_2Li_{1/2}Ni_{1/2}O_4$ and the Co^{III} analogue the diffraction pattern may be interpreted as generated from the partial pseudomerohedric (110) twin of the orthorhombic structure (space group $Ammm$, No. 65) but with tetragonal metric (1). In terms of the axis system of the first domain type A the second (type B) may be described in the space group $Bmmm$ (it should be noted that no transformation to the conventional $Cmmm$ setting is made, in order to keep the c-axis from the parent K_2NiF_4 structure). All main structure reflections (hkl: $h + k$, $h + l = 2n$) coincide for both domains. Using the SHELXL97 program package (5) the structure was refined as a (110) reflection twin with ordered Li and Co atoms within the a, b layers. All reflections compatible with A centering only were allotted to domain A, those compatible with B centering only to domain B, while the main structure reflections were assigned to both domains (6). In difference to the analogous solids $La_2Li_{1/2}Ni_{1/2}O_4$ and $La_2Li_{1/2}Co_{1/2}O_4$ (1) no significant contributions of "small" domains below the coherence length of the used radiation, which would require the additional introduction of disorder at the Li/Co metal sites, were observed. However, very weak diffuse streaks along c^* were additionally observed in this case, e.g., at the ± 101, ± 301, $\pm 2 \pm 11$, 0 ± 11 reciprocal lattice bars. The maxima at the allowed superstructure reflections were sharp and much stronger in intensity than the diffuse part of the diffraction pattern which showed no further maxima. Plots of the reciprocal lattice planes extracted from the IPDS data revealed that the intensities of the strongest main structure reflections, of the strongest superstructure maxima, and of the strongest diffuse streaks are 65,000, 4000, and 200, respectively. Thus, the indicated one-dimensional stacking disorder along the c-axis is of minor importance. The main part of the crystal shows a complete order between Li and Co on the octahedral sites within the limits of error. The twin refinement disregards the diffuse scattering and hence yields the idealized structure. Owing to the weak intensities of the superstructure reflections an unusual weighting scheme with $w = 1/1 + (0.1P)^2$ and $P = (F_o^2 + 2F_c^2)/3$ was used to prevent downweighting of the superstructure reflections. Therefore, the weighted wR_2 residual (0.28) is less meaningful in this case; also the extinction coefficient is rather large, leading to high residual electron densities (Table 1). The conventional R converged at 0.048. To reduce the correlations induced by the dominant pseudosymmetry and the twinning, the displacement factors of the Li, Co, and O atoms were kept isotropic and those of Li and Co were taken to be equal. With these restrictions, we achieve the
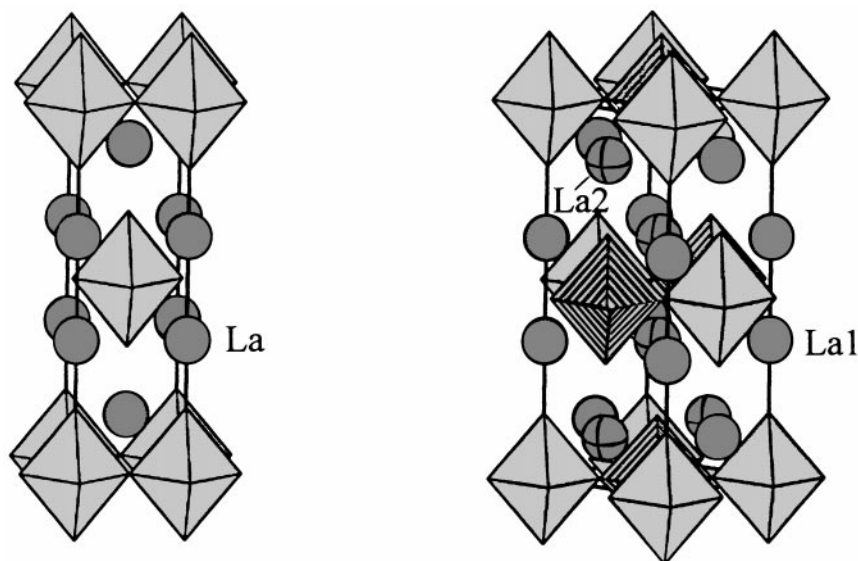
FIG. 1. Left: K$_2$NiF$_4$-type unit cell of La$_2$NiO$_4$ (space group $I4/mmm$, No. 139; lattice constants a_0, c_0). Right: Superstructure induced by cation ordering in the solids La$_2$Li$_{1/2}$M$_{1/2}$O$_4$ (unit cell of space group $Ammm$, No. 65, shifted by $\delta x = 1/2$ in respect to the atomic positions in Table 3 and with lattice constants $a = b = a_0\sqrt{2}$, $c = c_0$); lighter and darker shaded polyhedra are occupied by Li and Co, respectively.

most reliable refinement of the structural geometry and of the twin ratio. The latter was found to be 0.832(6), which is in good agreement with optical estimates from the reciprocal space plots. The La/Sr ratio was refined separately for both independent La sites (Table 2), with the difference being seemingly significant. The resulting stoichiometry of La$_{1.84}$Sr$_{0.16}$Li$_{1/2}$Co$_{1/2}$O$_4$ is in fair agreement with the EDX investigations of other crystals of the same preparation. More experimental details and the positional parameters are given in Tables 1 and 2, respectively. A more detailed description of the novel K$_2$NiF$_4$-type superstructure is given in Ref. (1).

III. DISCUSSION OF THE STRUCTURAL RESULTS

Important interatomic distances and angles are summarized in Table 3. The LiO$_6$ octahedra are distinctly tetragonally elongated parallel to the crystallographic c-axis, with Li–O spacings of 191.5(3) (4×) and 227(1) pm (2×)—similar to those in La$_2$Li$_{1/2}$Ni$_{1/2}$O$_4$ (192 and 231 pm). The X-ray single crystal analysis of the latter solid yielded the most reliable structural results in the series of compounds of the general type La$_2$Li$_{1/2}$$M^{III}_{1/2}O_4$, with M^{III} = Co, Ni, and Cu, described before (1). Slightly less elongated are the CoO$_6$ polyhedra, 186.4(3) (4×), 206.5(1) pm (2×), the spacings closely resembling those of La$_2$Li$_{1/2}$Co$_{1/2}$O$_4$, if the Li–O distances from the Ni^{III} solid are adopted ($\cong$186 and $\cong$205 pm) (1). The average Co–O spacing in La$_{1.84}$Sr$_{0.16}$Li$_{1/2}$Co$_{1/2}$O$_4$ is 193 pm, yielding, with $r(O^{2-}) = 140$ pm, an ionic radius of 53 pm for Co, which is even slightly smaller than the reported value for

low-spin Co^{III} (54.5 pm, in comparison with 61 pm for the high-spin configuration) (8). Thus, the Co–O distances definitely hint toward a t^6_{2g} configuration of Co^{III} and seem further to indicate the presence of a fraction of cobalt in the (+IV) oxidation state with a smaller radius than that of Co^{III}. The considerable elongation of both the LiO$_6$ and the CoO$_6$ octahedra can be traced back to lattice strains, e.g., to anisotropic contrapolarizing forces of mainly La^{III} on the oxygen ligator atoms (1).

The oxygen coordinations of La^{III}/Sr^{II} on the 1 and 2 positions are strongly distorted Archimedes antiprisms with one capped face. The average La^{III}–O distance reported for both sites in La$_2$Li$_{1/2}$Ni$_{1/2}$O$_4$ (261.5 pm) (1) corresponds exactly to the ionic radius of La^{III}, if again $r(O^{2-}) = 140$ pm is assumed (8). The respective La(Sr)–O spacings in La$_{1.84}$Sr$_{0.16}$Li$_{1/2}$Co$_{1/2}$O$_4$ are 260.5 and 261.5 pm for position 1 and 2, respectively (Table 3). Though within the standard deviations, the difference in distance seems to reflect a considerably larger Sr^{2+} fraction on site 2 (Table 2(a)). The ionic radius of Sr^{II} is about 10 pm larger than that of La^{III} (8), implying an expected increase of the averaged distance by about 1 pm, if 10 mol% of La^{III} is substituted by Sr^{II}. Otherwise the single La(Sr)–O spacings and the O–La(Sr)–O angles differ from those in La$_2$Li$_{1/2}$Ni$_{1/2}$O$_4$ by at most ± 6 pm and $\pm 4°$, respectively.

IV. THE ELECTRONIC STRUCTURES OF Co^{III} AND Co^{IV}

EPR and Optical Spectroscopy

The EPR spectrum of the pure cobalt(III) compound ($x = 0$) between 4 and 300 K shows exclusively the typical

TABLE 1
Measuring Conditions and Parameters for the X-ray Analysis of $La_{1.84}Sr_{0.16}Li_{1/2}Co_{1/2}O_4$

	Crystal data
Formula	$La_{1.84}Sr_{0.16}Li_{1/2}Co_{1/2}O_4$
Crystal size, mm^3	$0.014 \times 0.097 \times 0.138$
Absorption μ, mm^{-1}	25.94
Space group	*Ammm*, $Z = 4$
Lattice parameters, pm	
a	534.0(1)
b	535.0(1)
c	1262.1(2)
Temperature, K	293
D_c, g/cm^{-3}	6.67
	Data collection
Diffractometer	IPDS (Stoe) (4)
Radiation	Mo$K\alpha$ graphite monochromator (71.073)
Measuring mode	$\Phi = 0\text{--}200°$, $\Delta = 1°$, $D = 60$ mm, $t = 2$ min/Exp
Completeness	0.99
Theta range, °	3.2–27.9; $\pm h$, $\pm k$, $\pm l$
Reflections, total/used/uniques (1 domain)	3410/1687/268
	Computing
Refinement (5)	SHELXL-97
Atomic scattering factors	For neutral atoms; $\Delta f'$ and $\Delta f''$ from (7)
Absorption correction (4)	Numerical
Extinction correction (5)	$\varepsilon = 0.010(2)$
Refinement method	Full matrix least squares, $\sum w(F_o^2 - F_c^2)^2$ minimized
Number of parameters	21
$R_2(F^2)$, $R(F)$ (all refl.)	0.286, 0.0482
Goodness of fit	2.47
Max. ratio shift/esd	< 0.001
$\Delta\rho_{max/min}$, e/Å^3	4.7, −4.5

TABLE 2
Atomic Positions, (Equivalent) Isotropic Displacement Factors U [10^{-20} m^2 = Å^2] and Site Occupation Factors for $La_{1.84}Sr_{0.16}Li_{1/2}Co_{1/2}O_4$ (a), Anisotropic Displacement Factors of La^{III} and Sr^{II} (b)

Atom	Position[a]	x	y	z	s.o.f.	U
			(a)			
La1	4g	0	0	0.13518(4)	0.96(4)	0.0051(7)
Sr1					0.04(4)	0.0051(7)
La2	4h	0.5	0	0.36461(5)	0.88(4)	0.0052(7)
Sr2					0.12(4)	0.0052(7)
Li	2b	0	0	0.5	1	0.0045(6)
Co	2d	0.5	0	0	1	0.0045(6)
O1	8n	0.2553(6)	0.2486(6)	0	1	0.002(1)
O2	4g	0	0	0.3202(9)	1	0.019(2)
O3	4h	0.5	0	0.1636(8)	1	0.011(2)

Atom	U_{11}	U_{22}	U_{33}
		(b)	
La1(Sr1)	0.0051(9)	0.0070(9)	0.0031(8)
La2(Sr2)	0.0074(9)	0.0058(9)	0.0028(8)

[a] Erroneously, the Wyckoff notations for the space group *Bmmm* were given in Ref. (1) instead of those for *Ammm*.

isolated Co^{IV} polyhedra, overlaps a second component of the same type, which is broadened by weak dipolar coupling between several centers in a multication cluster. The simulation parameters are given in the caption of Fig. 2, and the resulting g- and hyperfine constants A (in 10^{-4} cm^{-1}) are summarized in

$$g_x = 2.442, \quad g_y = 2.237, \quad g_z \approx 0.8,$$

$$|A_z| \approx 30, \quad |A_y| < 10, \quad |A_x| = 107. \quad [2]$$

The spectrum is clearly orthorhombic, which may be readily explained by an inhomogeneous distribution of Li^I ions in the neighborhood of a paramagnetic Co^{IV} center because either vacancies on the Li positions or the presence of Li^I on

TABLE 3
Bond Lengths (pm) within the Metal−Oxygen Polyhedra in $La_{1.84}Sr_{0.16}Li_{1/2}Co_{1/2}O_4$

Li			Co	
Li–O1	191.5(3)	4×	Co–O1	186.4(3)
Li–O2	226.9(12)	2×	Co–O3	206.5(10)
La1(Sr1)			La2(Sr2)	
La1–O1	255.7(3)	4×	La2–O1	253.7(3)
La1–O2 (short)	233.6(1)	1×	La2–O3 (short)	253.7(1)
La1–O2	273.3(3)	2×	La2–O2	272.8(3)
La1–O3	269.4(2)	2×	La2–O3	269.9(2)

features of a cation with low-spin t_{2g}^5 configuration in a tetragonally elongated octahedral coordination (Fig. 2), as will be discussed below. Apparently the transition metal ion, which is predominantly in the EPR-silent low-spin Co^{III} state (t_{2g}^6), contains a certain fraction of low-spin cobalt(IV). This is in agreement with the experimental determination of the oxidation state, indicating a higher average value than (+III) and a smaller ionic radius than that of low-spin Co^{3+} (1). The EPR spectrum is nicely resolved in the $g_\perp$ region only at lower temperatures (Figs. 2a and 2b), with a hyperfine splitting into eight lines, caused by the nuclear spin I = 7/2 of ^{59}Co (100% abundance). The broad g_z signal at ≈ 0.8 is observed at higher temperatures, and the weak sharp line at the half-field position is probably due to a tiny percentage of interacting Co^{IV} polyhedra.

The 98 K spectrum could be fairly well simulated (Fig. 2c) with the assumption that one spectral component with resolved hyperfine-structure and narrow line width, due to
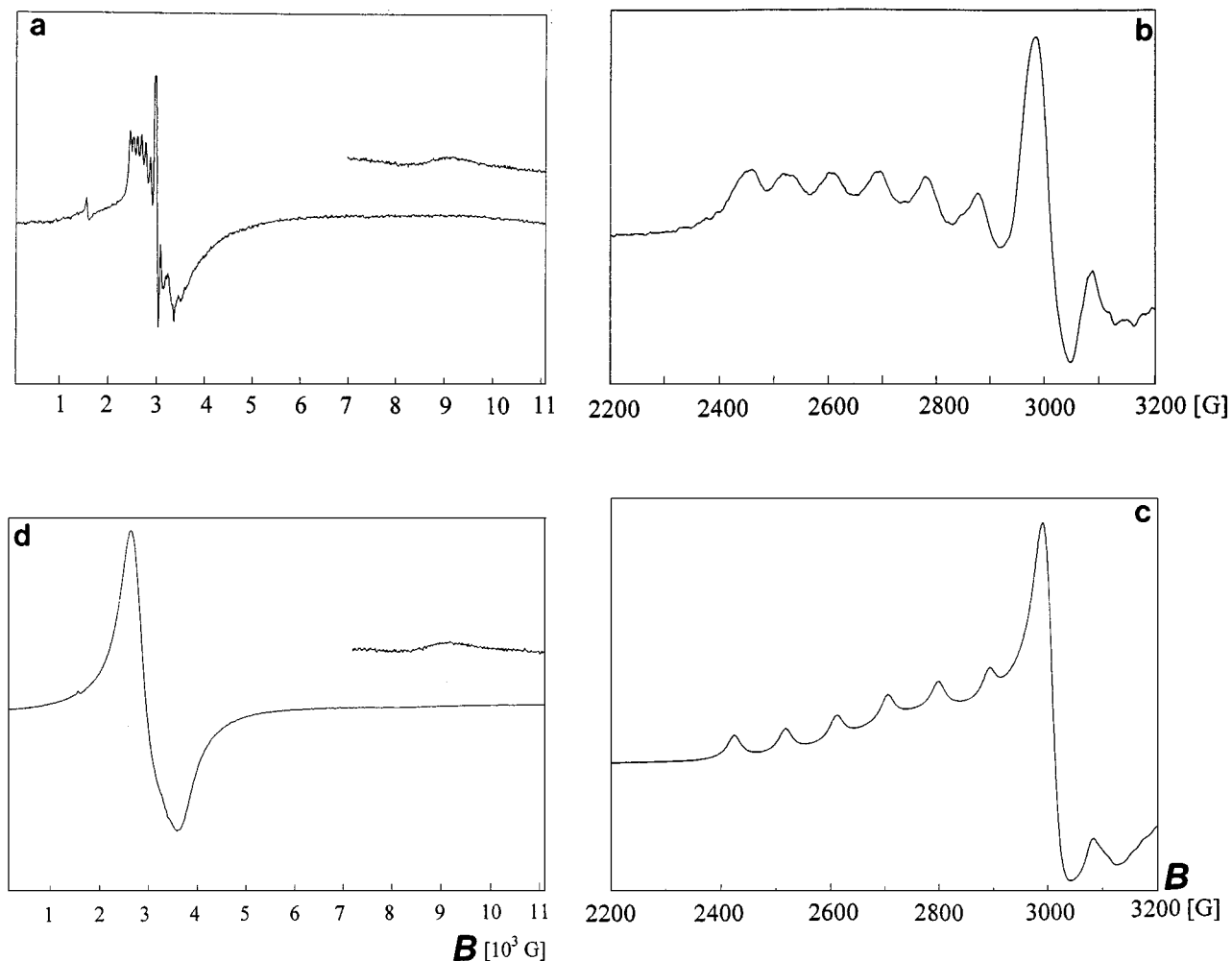
FIG. 2. X-band EPR powder spectrum of La$_2$Li$_{1/2}$Co$_{1/2}$O$_4$ at 98 K, with the weak signal around $g_z \approx 0.8$ shown amplified (a). The main signal is depicted in larger scale in (b), while (c) shows the corresponding simulated spectrum, resulting from the superposition of two spectra with the parameters: $g_x = 2.442$, $g_y = 2.237$; $|A_x| = 107 \times 10^{-4}$ cm^{-1}, $|A_y| = 10 \times 10^{-4}$ cm^{-1}, half width $\Delta H = 9$ and 15 G, respectively, and $g_x = 2.44$, $g_y = 2.24$; $|A_x| = |A_y| \cong 10 \times 10^{-4}$ cm^{-1}, $\Delta H = 100$ and 15 G (intensity ratio 1:3). Spectrum d (108 K) refers to Sr$_{0.2}$La$_{1.8}$Li$_{1/2}$Co$_{1/2}$O$_4$ with about 40 mol% Co^{IV}.

a tiny fraction of the Co sites have to be assumed for reasons of charge compensation (La$_2$Co$_{1/2}$Li$_{1/2-\delta'}$O$_4$ (δ': fraction of Co^{IV}) or La$_2$(Co$_{1/2-\delta}$Li$_\delta$)Li$_{1/2}$O$_4$ ($\delta = 2\delta'$), respectively). Increasing the Co^{IV} concentration in the mixed crystal series La$_{2-x}$Sr$_x$Li$_{1/2}$Co$_{1/2}$O$_4$ leads to a washing out of the hyperfine structure and a broadening of the spectrum, without destroying the main spectral features (Fig. 2d). It cannot be decided, however, if the orthorhombic symmetry component is retained or whether it has changed its magnitude. From the broad EPR spectrum of the compound with $x = 0.5$, a $g_\perp$-value of 2.32 was estimated (3, 9), similar to the one reported here. The Q-band spectrum of La$_2$Li$_{1/2}$Co$_{1/2}$O$_4$ confirms the given analysis. As expected, the g_x signal—resolved into eight hyperfine lines—and the narrow g_y signal are well separated at the higher measuring

frequency. Also this spectrum could be fairly well simulated using very similar parameters to those given for Fig. 2c. The energy splitting of the octahedral $^2T_{2g}$ ground state of a t_{2g}^5 cation by a tetragonal field (D_{4h} elongation) and LS coupling is shown in Fig. 3. It corresponds to that of the t_{2g}^1 configurated Ti^{III} ion (10), but with a reversed sign of the tetragonal-field splitting parameter δ_2 and the effective spin-orbit coupling constant λ (11). The g values arising from the $_a\Gamma_7$ ground state are given in Eq. [3], if higher-order contributions from excited states are neglected.

$$g_\| = |g_o \cos 2\phi - k(1 - \cos 2\phi)|$$

$$g_\perp = |1/2\,g_o(1 + \cos 2\phi) - \sqrt{2}k \sin 2\phi| \qquad [3]$$

$$[\cos 2\phi = (3\delta_2 + 1/2\,\lambda)/W; \ \sin 2\phi = \sqrt{2}\lambda/W].$$

k is the orbital reduction (or covalency) factor, which reduces the LS coupling constant λ_0 of the free Co^{4+} ion ($\lambda_0 \cong -650 \text{ cm}^{-1}$) by covalency to the effective value $\lambda = k \cdot \lambda_0$, and W is defined in Fig. 3 (caption). With the condition $|\lambda| = 1.95 \, \delta_2$ and a covalency parameter of reasonable magnitude for a cation in a high oxidation state ($k = 0.65$), one obtains $g_{\parallel} = 0.79$ and $g_{\perp} = 2.35$, in excellent agreement with the experimental values, if the average of g_x and g_y (Eq. [2]) is defined as $g_{\perp}$. The derived parameter set—$3 \, \delta_2 = 650 \text{ cm}^{-1}$, $\lambda = -425 \text{ cm}^{-1}$—places the Γ_6 and $_b\Gamma_7$ terms at $\cong 1000$ and $\cong 750 \text{ cm}^{-1}$, respectively, above the $_a\Gamma_7$ ground state. The spectroscopically indicated tetragonal elongation of the CoO_6 octahedra corresponds to the structural finding. It is mainly caused by lattice strains (see Section III), but may have a small Jahn–Teller contribution due to the presence of Co^{IV} as well. The octahedral $^2T_{2g}$ ground state of Co^{IV} is the subject of vibronic coupling, demanding an elongation in order to induce an orbital singlet to be the lowest split state. Because the t_{2g} MO's are only π-antibonding, the energy effect accompanying the structural distortion is rather small, with a ground state splitting of only about 1000 cm^{-1}.

The optical spectrum of the brown solid $La_2Li_{1/2}Co_{1/2}O_4$ shows a d–d transition at $\cong 13,500 \text{ cm}^{-1}$, overlapping the slope of the charge-transfer region, which reaches its highest intensity around $22,000 \text{ cm}^{-1}$ (1). The latter region has distinctly shifted to lower energies ($\cong 15000 \text{ cm}^{-1}$) in the case of the Co^{III}/Co^{IV} compound, as expected if the oxidation state of the involved transition metal ion increases, leading to a brownish black color. The d–d band of Co^{III} is still visible as a superimposed feature, however. While Co^{IV} is definitely low-spin configurated, the question whether Co^{III} occurs in the high- or low-spin configuration in ceramic oxides is still controversely discussed. The structural results and data from ligand field spectroscopy for isolated $Co^{III}O_6$ octahedra in oxide ceramics, such as $La_2Li_{1/2}Co_{1/2}O_4$ (1), give evidence for a low-spin t_{2g}^6 configuration. They also indicate that the value of the ratio 10Dq/B between the ligand field parameter and the Racah parameter of interelectronic repulsion is close to the critical value for the spin crossover. Low-lying excited quintet states, deriving from $t_{2g}^4 e_g^2$, may hence be expected. X-ray absorption spectroscopy is the method of choice to obtain additional information regarding the electronic structure of Co^{III}.

XANES Spectroscopy

The cobalt XANES spectrum of $La_2Li_{1/2}Co_{1/2}O_4$ taken at the $Co-L_{2,3}$ thresholds (Fig. 4b) is similar to that of $LaCoO_3$ or $LiCoO_2$ recorded at 300 K (12, 13) and indicative of low-spin Co^{III}. Here, the lower-energy and the weaker higher-energy part originate from the excitation of a $2p_{3/2}$
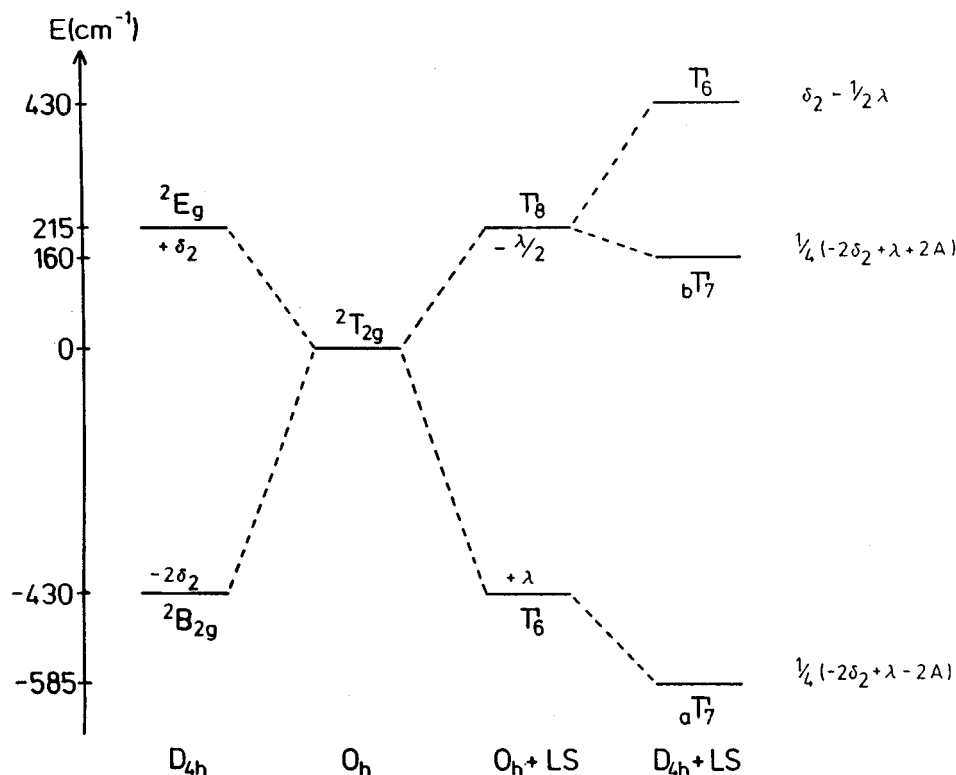

FIG. 3. Term energies of a t_{2g}^5 cation in a tetragonally elongated octahedral ligand field with LS coupling included [$W = \{9\delta_2^2 + 3\delta_2\lambda + 9/4\lambda^2\}^{1/2}$; $\lambda = k \cdot \lambda_o < 0$]. The scale corresponds to the condition: $\lambda = -2\delta_2 = -430 \text{ cm}^{-1}$.
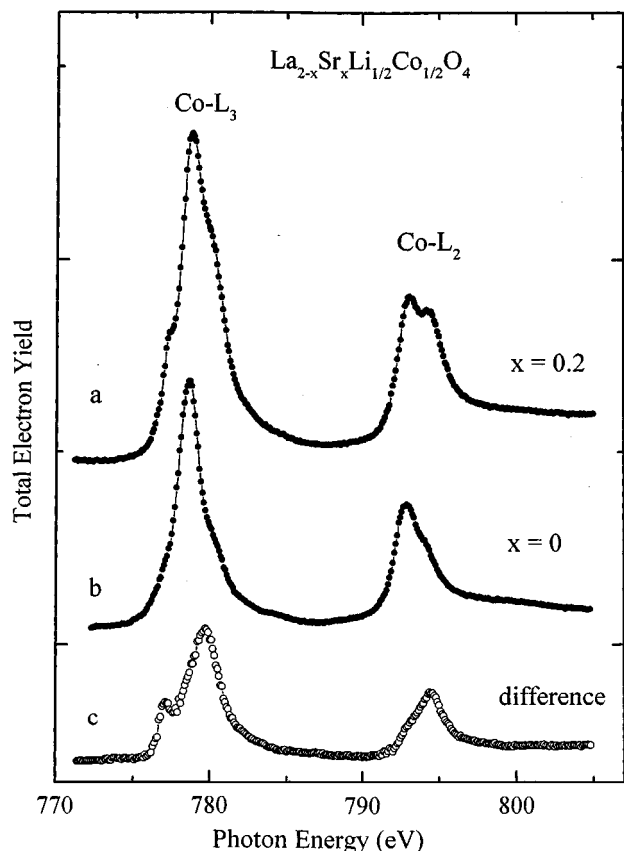
FIG. 4. Co–L$_{2,3}$ XANES spectra of cobalt in mixed crystals La$_{2-x}$Sr$_x$Li$_{1/2}$Co$_{1/2}$O$_4$ with (a): $x = 0.2$ (Co^{III}/Co^{IV}) and (b) $x = 0$ (Co^{III}); a Lorentzian lifetime broading of 0.5 eV for each $3d$ configuration and a Gaussian broading of the same magnitude have been assumed. In (c) the difference spectrum between (a) and (b) (appropriately weighted) is shown (Co^{IV}).

and a $2p_{1/2}$ electron, respectively, to an empty $3d$ state close to E_F. The shoulder around 777 eV, which is seen in the spectra of LaCoO$_3$ and LiCoO$_2$ as well, gets very weak after scraping and has to be ascribed to Co^{II} impurities. Switching to the spectrum of La$_{1.8}$Sr$_{0.2}$Li$_{1/2}$Co$_{1/2}$O$_4$ (Fig. 4a) a pronounced enhancement in particular of the distinct shoulders in the higher-energy slopes of the L_3 and L_2 absorption curves is observed. This is apparently due to the presence of Co^{IV}, keeping in mind that the main peaks are expected to shift to higher energy with increasing oxidation state (14, 2). The approximate intrinsic Co^{IV} spectrum (Fig. 4c) is obtained by subtracting the appropriately weighted Co^{III} spectrum b from the Co^{III}/Co^{IV} spectrum a and is indeed very similar to that reported for SrCoO$_3$ (14). A spectral weight of 36% Co^{IV} is deduced rather close to the value resulting from the X-ray investigation.

There have been difficulties in the past reproducing the experimentally observed multiplet structure of oxidic Co^{III} solids precisely, even when taking covalency contributions

and high (or intermediate) spin admixtures to the ground state into account (12, 13). In the present study we have performed charge-transfer multiplet calculations (2) in order to simulate the spectrum. The program package includes an atomic multiplet (15), a group theory (16), and a charge-transfer program (17). The ground state wave function of Co^{III} is given in Eq. [4], adopting the underlying (13–15) bonding concept

$$\Phi_g = \alpha_0 \,|3d^6\rangle + \beta_0 \,|3d^7\underline{L}\rangle \qquad (\alpha_0^2 + \beta_0^2) = 1. \quad [4]$$

Here $\underline{L}$ denotes an oxygen $2p$ hole, and α_0 and β_0 are configurational mixing coefficients. Covalency is allowed for by the linear combination of the ionic $3d^6$ with a configuration, where one ligand electron is transferred to the metal atom. If a large charge-transfer gap ($\Delta = 6$ eV), equivalent to weak covalency, is chosen, a theoretical spectrum very similar to that resulting from an atomic multiplet calculation results, in which the splitting between the main peak and the higher-energy shoulder is too distinct with respect to the experiment in both the L_3 and the L_2 spectral regions (Fig. 5). A much better fit results for $\Delta = 3.5$ eV, the ligand
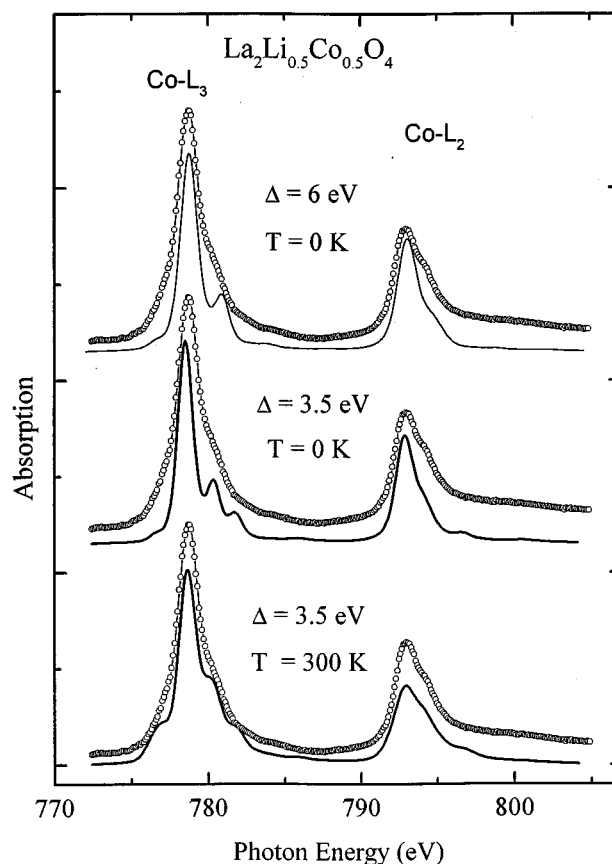

FIG. 5. Calculated spectra of octahedrally coordinated Co^{III} ions (solid lines) in comparison to spectrum (b) in Fig. 4 (dotted curve); the simulation parameters are cited in the text.

field and interelectronic repulsion parameters being $10Dq = 1.6$ eV (in very good agreement with the value, suggested from ligand field considerations (1)) and $U_{cd} - U_{dd} = 2$ eV, respectively (see (2) for theoretical details and definitions). The fit is further improved when assuming that an excited term resulting from the $t_{2g}^4 e_g^2$ ($S = 2$) configuration is in thermal reach (at 28 meV). Without taking the cited numerical value of the quintet–singlet separation energy too seriously, the XANES spectra confirm nicely the presence of a low-spin t_{2g}^6 ($S = 0$) ground state for Co^{III} in $La_{2-x}Sr_xLi_{1/2}Co_{1/2}O_4$ mixed crystals, but with ligand field and interelectronic repulsion parameters close to those characteristic for the spin-crossover. A Boltzmann distribution over the t_{2g}^6 ground state and close-lying excited $S = 2$ states may also explain the temperature dependence of the $LaCoO_3$ XANES spectrum between 200 and 500 K. Here, a transition to a high-spin ground state has been postulated at even higher temperature (13). The percentage of the $3d^7\underline{L}$ contribution to the ground state (Eq. [4]) derived from the best fit parameters for $La_2Li_{1/2}Co_{1/2}O_4$ is 28%, corresponding to $\alpha_0 \cong 0.85$. For the perovskite $LaCoO_3$, where more pronounced electron delocalization effects due to corner-connected $Co^{III}O_6$ octahedra in three dimensions are expected, more covalent Co^{III}–O bonds result from band-structure and cluster calculations (18). In these calculations, the configurations $3d^6$, $3d^7\underline{L}$ and $3d^8\underline{L}^2$ contribute with 62, 36, and 2%, respectively, to the ground state. The covalency contributions for Ni^{III} and Cu^{III} in the solids $La_2Li_{1/2}M_{1/2}^{III}O_4$ are considerably larger than for Co^{III}, namely 43% ($3d^8\underline{L}$) and 70% ($3d^9\underline{L}$), respectively (2). Translating the obtained distribution percentages of the antibonding e_g electrons within the M^{III}–O bonds into the one-electron MO description of Eq. [1], we estimate mixing coefficients α around 0.9_5, 0.9, and 0.8 for Co^{III}, Ni^{III}, and Cu^{III}, respectively. Apparently the Co^{III}–O bond is considerably more ionic than, in particular, the Cu^{III}–O bond. The given numbers nicely correlate with the third ionization energies of the transition metals, which increase from 33.5 eV for cobalt via 35.2 eV for nickel to 36.9 eV for copper (17).

Electron-correlation effects are of only minor influence, if the XANES spectra at the oxygen K-edge are considered. Here, band-structure calculations are rather efficient (2, 12–14). Therefore, such measurements are usually applied, when O–$2p$ holes induced by covalence are explored. The OK XANES spectrum of $La_2Li_{1/2}Co_{1/2}O_4$, displayed in Fig. 6a, shows a rather narrow peak A at 529.6 eV, which provides the most interesting information concerning the electronic structures of cobalt and oxygen, and further broad features above 531 eV attributed to lanthanum $5d$ and cobalt $4s,p$ bands (12–14). The former pre-edge absorption is assigned to a $\underline{1s}(O)3d^7(Co)$ final state. Though the $1s \rightarrow 3d$ transition is parity-forbidden, it gains intensity by the admixture of oxygen $2p$ orbitals due to covalence. Thus
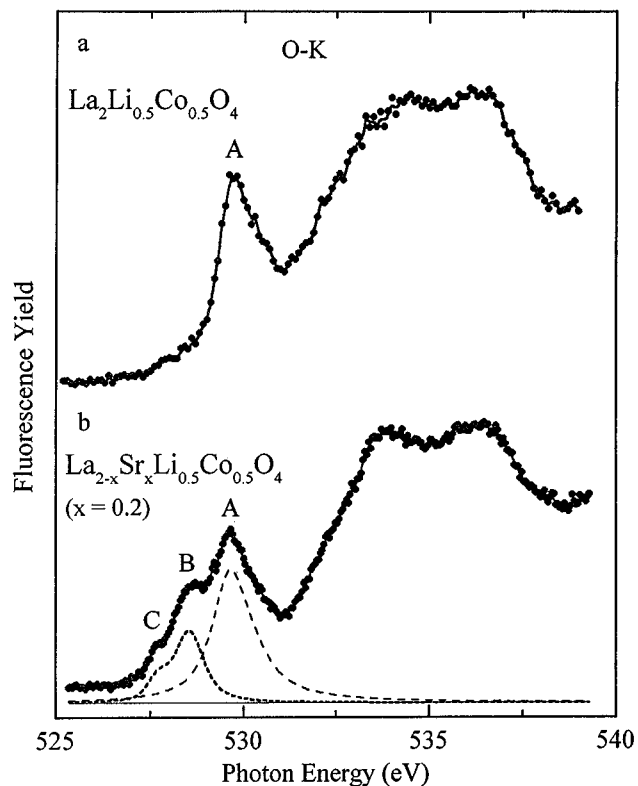

FIG. 6. OK XANES spectra of (a) Co^{III} in $La_2Li_{1/2}Co_{1/2}O_4$ and (b) Co^{III}/Co^{IV} in $La_{1.8}Sr_{0.2}Li_{1/2}Co_{1/2}O_4$. For the latter compound, the spectral weights of Co^{III} (dashed curve) and Co^{IV} (dotted curve) are given in the pre-edge region.

the intensity of the pre-edge peak reflects the fraction of electron holes in the oxygen $2p$ band and is proportional to the square of the configurational mixing coefficient β_0 in Eq. [4]. The appearence of a single absorption band matches with low-spin Co^{III} as the origin, because only e_g^* MOs can be occupied by the excited $O1s$ core electron.

Proceeding from the mixed crystal $La_{2-x}Sr_xLi_{1/2}Co_{1/2}O_4$ with $x = 0$ (Fig. 6a) to that with $x \cong 0.2$ (Fig. 6b) two new features B and C evolve, shifted to lower energies with respect to A by 1.1 and 2.1 eV, respectively, and readily assigned to Co^{IV}. These shifts are similar to those observed for nickel and copper in oxide ceramics, when the oxidation states increase (2). The peaks C and B correspond to $\underline{1s}\,3(t_{2g}^6)$ and $\underline{1s}\,3(t_{2g}^5 e_g^1)$ final states with a splitting of $\cong 1$ eV, which should roughly represent the ligand-field parameter $10Dq$ for Co^{IV}. This value is much smaller than that expected for Co^{IV} ($10Dq \approx 3$ eV). One has to consider, however, that contributions from interelectronic repulsion and from the symmetry effect caused by the distinct tetragonal elongation of the CoO_6 polyhedra may play an important role in this apparent reduction. Thus the energy of the lowest multiplet term $^3T_{1g}$ resulting from the excited $t_{2g}^5 e_g^1$ configuration is smaller than $10\,Dq$ by nearly 1 eV relative to $^1A_{1g}(t_{2g}^6)$; see

the Tanabe–Sugano diagram of d^6 (19) for more details. On the other hand, the tetragonal field splitting of the σ-antibonding e_g MO is expected to be considerable, because already the only π-antibonding t_{2g} MO splits by about $1000\,\text{cm}^{-1}$ (see Fig. 3). After all the assignment of the prepeak B as being correlated with $1s3(t_{2g}^5 e_g^1)$ is only approximate.

It has recently been proposed that the ground state of Co^{IV} in SrCoO$_3$ might be of intermediate spin type (14). While such behavior cannot be excluded with certainty, if interconnected Co^{IV}O$_6$ octahedra with the possibility of itinerant electrons are present, the EPR results unambiguously yield a low-spin ground state for Co^{IV} in the solid La$_{1.84}$Sr$_{0.16}$Li$_{1/2}$Co$_{1/2}$O$_4$, where the Co^{IV}O$_6$ polyhedra are isolated from each other in the ordered K$_2$NiF$_4$ matrix. This observation is expected, because already Co^{III} with a significantly lower ligand field parameter is low-spin in this type of solids.

V. SUMMARY AND CONCLUSIONS

The solids La$_{2-x}$Sr$_x$Li$_{1/2}$Co$_{1/2}$O$_4$ with $x = 0$ (1) and $x \cong 0.2$ crystallize in an orthorhombic K$_2$NiF$_4$-type superstructure with an ordered distribution of the lithium and cobalt ions over the octahedral sites (space group $Ammm$, No. 65). The single crystal X-ray analysis reveals an enlargement of the basic K$_2$NiF$_4$ unit cell in the (001) plane according to $a = b = a_0\sqrt{2}$. The presence of very weak streaks along c^* indicates tiny stacking disorder contributions parallel to [001]. The LiO$_6$ and CoO$_6$ octahedra show distinct tetragonal elongations due to anisotropic lattice strains.

The Co^{III}O$_6$ and Co^{IV}O$_6$ polyhedra lie isolated in the lattice (about 60 and 40 mol%, respectively, in the compound with $x \cong 0.2$), so that the electronic properties of the transition metal ions can be studied without significant disturbance by metal–metal interactions and low-lying intervalence bands. Both Co^{III} and Co^{IV} occur in the low-spin configuration, with $^1A_{1g}$ (t_{2g}^6) and $^2T_{2g}(t_{2g}^5)$ ground states, respectively. The latter is split by about $1000\,\text{cm}^{-1}$ by the tetragonal ligand-field component, and in the former case excited high-spin states in thermal reach with respect to the $^1A_{1g}$ ground term seem to be present, which might be populated at higher temperatures. While EPR spectroscopy yields very detailed informations on the electronic structure of the paramagnetic Co^{IV} center, XANES spectroscopy is the method of choice to characterize the electronic properties of the diamagnetic Co^{III} cations. The Co^{III}–O bond is

essentially ionic ($\alpha \cong 0.95$), with the covalency increasing distinctly by the substitution of Co^{III} by Ni^{III} ($\alpha \cong 0.9$) and especially by Cu^{III} ($\alpha \cong 0.8$) (2) in the same class of compounds, La$_2$Li$_{1/2}M_{1/2}^{III}$O$_4$. Following the arguments and calculations for the Co^{IV}–O bond in SrCoO$_3$ (18), a MO mixing coefficient is estimated ranging between those of Ni^{III} and Cu^{III} in La$_2$Li$_{1/2}M_{1/2}$O$_4$.

REFERENCES

1. S. A. Warda, W. Pietzuch, G. Berghöfer, U. Kesper, W. Massa, and D. Reinen, *J. Solid State Chem.* **138,** 18 (1998).
2. Z. Hu, G. Kaindl, S. A. Warda, D. Reinen, B. G. Müller, and F. de Groot, *Chem. Phys.* **232,** 63 (1998).
3. G. Demazeau, B. Buffat, M. Pouchard and P. Hagenmüller, *J. Solid State Chem.* **54,** 389 (1984).
4. Stoe: Program package for X-ray diffraction, version 2.79, Stoe IPDS; Darmstadt, Germany (1997).
5. G. M. Sheldrick: SHELXL-97, Release 2, "Program for the Refinement of Crystal Structures," University of Göttingen, Germany (1996).
6. F. Hahn, W. Massa, TWINXL, Program zur Aufbereitung von Datensätzen verzwillingter Kristalle, Marburg, 1996.
7. "International Tables for Crystallography," (A.J.C. Wilson, Ed.), Vol. C. *Kluwer Academic*, Dordrecht, 1992.
8. R. D. Shannon, *Acta Crystallogr, A* **32,** 751 (1976).
9. B. Buffat, G. Demazeau, M. Pouchard, J. M. Dance, and P. Hagenmüller, *J. Solid State Chem.* **50,** 33 (1983).
10. R. Ameis, S. Kremer and D. Reinen, *Inorg. Chem.* **24,** 2751 (1985).
11. B. N. Figgis, *Trans. Faraday Soc.* **57,** 198, 204 (1961).
12. M. Abbate, J. C. Fuggle, A. Fujimori, L. H. Tjeng, C. T. Chen, R. H. Potze, G. A. Sawatzky, H. Eisaki, and S. Uchida, *Phys. Rev. B* **47,** 16124 (1993).
13. Frank de Groot, Doctrol Thesis, University of Nijmegen, 1991.
14. R. H. Potze, G. A. Sawatzky, and M. Abbate, *Phys. Rev. B* **51,** 11501 (1995).
15. T. Crown, "The Theory of Atomic Structure and Spectra," University of California Press, Berkeley, 1981.
16. P. H. Butler, "Point Group Symmetry, Applications, Methods and Tables," Plenum Press, New York, 1981.
17. K. Okada, A. Kotani, and B. T. Thole, *J. Electron Spectrosc. Relat. Phenom.* **58,** 325 (1997).
18. M. Abbate, R. H. Potze, G. A. Sawatzky, and A. Fujimuri, *Phys. Rev. B* **49,** 7210 (1994).
19. J. S. Griffith, "The Theory of Transition Metal Ions," p. 261, 414, 415. Cambridge University Press, Cambridge, UK, 1971.